LBL-9651

CONF-7909130--1

Lawrence Berkeley Laboratory
UNIVERSITY OF CALIFORNIA

# Physics, Computer Science & Mathematics Division

Presented at the Conference on Advances in Radiation Protection and Dosimetry in Medicine, International School of Radiation Damage and Protection, Erici, Sicily, September 16-26, 1979; also to be published in the Proceedings of the Conference

## DETECTORS FOR RADIATION DOSIMETRY

Victor Perez-Mendez

September 1979

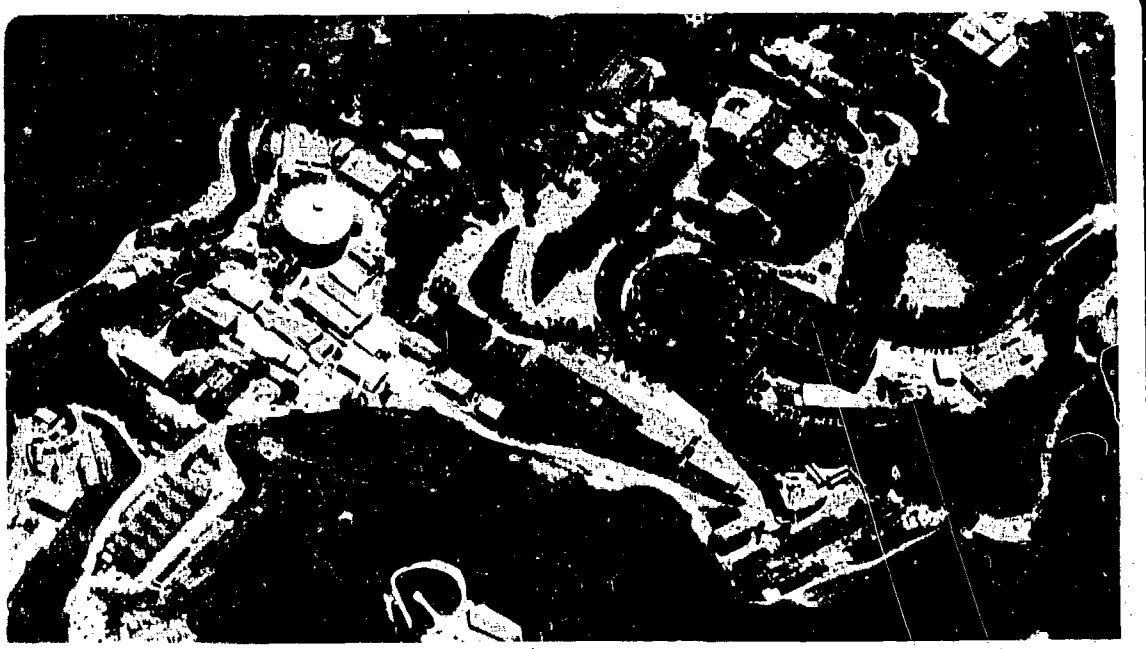

Prepared for the U.S. Department of Energy under Contract W-7405-ENG-48

# DETECTORS FOR RADIATION DOSIMETRY



Victor Perez-Mendez

Lawrence Berkeley Laboratory

Berkeley, CA 94720

## INTRODUCTION

In previous years Radiation Dosimetry in Medicine was concerned mainly with measuring doses produced by x-rays, gamma rays and electrons. These radiations have the common feature that their R.B.E. ≈ 1, and they can be monitored by the same types of detectors.

More recently, we have had to contend with measuring fluxes and doses produced by the radiations now coming into use in Radiation Therapy. These are heavy and light ions (Argon, protons), negative pions and neutrons.

The heavy ions, light ions and pions have the common feature that they are charged; their R.B.E. is a function of velocity and charge, and they produce some sort of Bragg Peak. The negative pions have the additional complication (and potential) of star formation when captured at low energies or at rest. Neutrons pose different problems since they are uncharged. Their effective R.B.E. depends on the energy, and since it is due to the recoils and secondary interactions of heavy charged particles produced in matter, it depends on the material through which they pass.

Health physicists have had to monitor the doses to personnel working in the vicinity of accelerators and reactors and have developed various detectors for monitoring the fluxes of these particles and measuring their dose to personnel working at the various installations. The material presented here draws heavily on the literature and practice of Health Physics technology. For completeness I will review briefly various detectors used in dosimetry and beam monitoring for x-rays and electrons, since their use also extends, with

Table I. Applications of Radiation Detectors

1) X-Rays, Gamma Rays, Electron Detectors
   a) Ionization Chambers
   b) Proportional and Geiger Counters
   c) Thermoluminescent Detectors
   d) Radioluminescent Glasses

2) Heavy- and Light-Ion Detectors
   a) Ionization Chambers
   b) Proportional and Geiger Counters
   c) Track Detectors

3) Pion Detectors
   a) Ionization Chambers
   b) Proportional and Geiger Counters

4) Neutron Detectors
   a) $BF_3$ Counters (Thermal Neutrons), $^3He$ Counters (Fast Neutrons)
   b) Plastic-Moderated Counters, Bonner Spheres
   c) Fission, Ionization, and Proportional Counters

5) General Detectors
   a) Scintillation Counters
   b) Solid State Detectors

slight modifications and different calibrations, to the other forms of radiation.

In Table I I have listed the most widely used detectors for monitoring beam fluxes and their applicability to the various types of radiations.

## GAS-FILLED DETECTORS

As noted in Table I, gas-filled detectors, i.e. ionization chambers, proportional counters and Geiger counters, are used in detecting and measuring the dose delivered to various objects by all the forms of radiation discussed here. In various situations the properties of the basic detector, i.e. ionization chamber or proportiona counter, are modified by the gas filling and by the surrounding material to make it suitable for the specific radiation in question.

### Ionization Chambers: General Properties

The unit of x-ray intensity, Roentgen, is defined in such terms

that it is conveniently measured by an air-filled ionization chamber. One Roentgen = "the quantity of x or gamma radiation such that the associated corpuscular emission per 0.001293 g of air produces in air ions carrying one unit of electrostatic electricity of either sign." (0.00293 g of air = 1 cc at N.T.P.) Note that the definition of Roentgen cannot be used for electrons or other forms of radiation.

Ionization chambers are often used for the following two purposes: 1) to measure and monitor the collimated flux of radiation incident on an object; 2) to sample, with as little perturbation as possible, the energy deposited locally at various points within an object which is being radiated. The electrical principles of operation of ion chambers for these two objectives are the same: the detailed shape, gas filling and materials of construction for these two are quite different.

A typical chamber for beam flux measurement is shown in Figs. 1b and 1c. The chamber is a parallel plate device whose sensitive area is larger than the collimated beam flux cross section. A chamber of this general shape can be used to monitor x-ray, gamma ray, heavy and light ion, pion and neutron beam fluxes. In general, the wall material thickness and gas volume should be thin enough so that the ion chamber, when placed in a beam as shown in Fig. 1a, interacts to a minimal extent with the beam, i.e. does not change its energy distribution or produce appreciable secondary particles.

The electrical characteristics of a chamber used to monitor heavy and light ion beams at LBL are shown in Fig. 1b, which can serve to explain the principles involved, including the use of guard ring electrodes to prevent collection of leakage currents. The thin windows (1) are the enclosure of the gas-filled region which can be filled to a higher pressure than atmospheric, and hence these windows can bulge outwards. The electrical collection part of the chamber consists of the two gold-plated (plated areas 2, 3, 4) plastic foils and the thin metal foil in the center. The high voltage (positive or negative) is connected to the central foil. The sensitive region of the chamber (B) is that between the metallic areas (3) on the plastic foils facing the high voltage foil (see Figs. 1b, 1c). All the metallized areas on the foils are at ground potential; the only ones which are read out are the central areas (3) which define the sensitive volume. The plated areas (2) and (4) at ground potential serve as guard rings to collect various leakage currents. Platings (4) receive the leakage currents across the insulators from the central high-voltage foil to ground. The metallic layers (2) on the plastic foils facing the gas envelope windows collect the ionization current produced in the gas volumes (A).

Fig. 1c shows a further elaboration in the structure of such a chamber: by dividing the sensitive region into a series of

concentric rings, each connected to a separate electronic charge integrator, it is possible to monitor continuously the beam distribution profile, assuming it is spherically symmetric. An alternative arrangement, useful for centering the beam, is to divide the central area into four independent quadrants.

Fig. 1d shows the charge collection voltage plateau typical of such a chamber. In the plateau region the electric field is high enough to drift electrons (or negative ions) and positive ions to their respective collectors with minimal recombination. Since the drift velocity of electrons is 10-1,000 times faster than the drift velocity of negative ions, the recombination probability is smaller in gases which are not electronegative and hence tend to produce very few negative ions, i.e. nobel gases (He, Ne, Ar, Kr, Xe) $N_2$, $CO_2$, $CH_4$, etc.

At very high beam fluxes, even in these gases, space-charge effects become sufficiently large, so that electron-ion recombination becomes appreciable and the full charge is not collected. At these beam levels it then becomes necessary to use other beam monitoring devices, such as the Secondary Electron Monitor (S.E.M.) described below (Fig. 2). These high fluxes can occur in heavy-ion, light-ion and pion producing accelerators in which high peak intensity fluxes occur, due to the pulsed characteristics of the machines when running in low duty cycle conditions. The S.E.M. consists of a series of metallic electrodes placed in a good vacuum ($10^{-6}$ torr) container. Charged particles traversing these foils eject secondary electrons from the foil surfaces. The current produced by these secondary electrons can be collected and recorded in the same manner as the ionization chamber currents. For a given beam flux, the S.E.M. currents are 10-1,000 times smaller than those of a comparable ionization chamber. In a good vacuum, the only charges present are electrons, hence problems due to ionic recombinations do not arise and any non-linearity effects are due to space-charge effects alone. This problem does not occur in practice, since it is always possible to raise the collector voltage to a point where the space-charge non-linearity is reduced to a negligible value for any given peak beam intensity.

## Calibration of Ionization Chambers as Charged Particle Beam Monitors

In principle, a knowledge of the L.E.T. of the incident particles, of W (the energy loss in producing a single-ion pair in the gas), and of the width of the sensitive region of the chamber is sufficient to calculate the flux of charged particles traversing the ion chamber as a function of the collected charge. In practice, there are a number of additional variables whose specific effect is difficult to estimate precisely. For instance, the pion beams

Table II. Summary of Measured $^{12}C \rightarrow {}^{11}C$ Cross Section

| Particle Energy (MeV/A) | Cross Section (millibarns) | Beam Intensity (ions/pulse) |
|---|---|---|
| 400 | 63.5 | $2.5 \times 10^4$-$1.2 \times 10^5$ |
| 1,050 | 57.4 | $4.0 \times 10^4$-$1.5 \times 10^5$ |
| 2,100 | 60.9 | $4.7 \times 10^4$-$1.5 \times 10^5$ |

always contain variable numbers of electrons and muons which have different L.E.T. than the pions. Again, the heavy ion beams may be accompanied by small numbers of ions in different charge states produced by scattering from the beam slits.

The general procedure has been to calibrate these chambers against some reaction whose cross section is known. Proton beam fluxes can be calibrated by putting a thin foil of $CH_2$ in the beam and measuring the yield of elastically scattered protons in a coincidence scintillator counter telescope, which detects the incident and recoil protons. Another reaction which has been used to calibrate beam flux detectors is the yield of $^{11}C$ from $^{12}C$ targets exposed to various ion beams from protons to Argon ions. The $^{11}C$ activity is counted with a calibrated NaI crystal. The cross section for Argon ions for this reaction, as measured by the Health Physics Group at the Lawrence Berkeley Laboratory, is shown above in Table II.

Ionization Chambers: X-Ray and Gamma Ray Beam Monitors

The beams used in medical practice are those produced by diagnostic x-ray machines (100-250 kVp), $^{60}Co$ or other radioisotope sources, and Radiotherapy electron linear accelerators (4-35 MeV).

For x-ray sources in the diagnostic range, it is possible to construct air equivalent ionization chambers which are absolute monitors in the sense that their collection efficiency satisfies the definition of the Roentgen. Two different geometrical approaches are possible, as shown in Fig. 3. In the first case, one has a sensitive volume defined by guard rings with a large column of air in

front and back so that equilibrium is achieved between the charge produced by x-ray interactions inside and outside the boundaries of the sensitive volume.

An alternative approach to air equivalent chambers is to use the Bragg-Gray prescription, in which a wall material of the appropriate density and appropriate average Z composition is used; this wall is made thick enough so that equilibrium is achieved between the air volume and wall interactions. This is shown in Fig. 3b. The minimum thickness of wall material needed for the equilibrium conditions is given in the table in Fig. 3c. A small-volume ionization chamber used for measuring the dose distribution within a given tissue volume is shown in Fig. 3d. The bakelite wall of the sensitive volume satisfies the Bragg-Gray condition. It is coated with a thin graphite layer on the inside to make it conducting.

Fig. 4 shows the use of a thimble chamber in measuring the dose distribution within a phantom. The total radiation flux incident on the phantom is monitored by a parallel-plate ionization chamber, as discussed previously. Fig. 4b shows the relationship between Roentgens (a unit of fluence) and rads (a unit of absorbed energy) for various materials of biological interest. Fig. 4c shows the number of photons/$cm^2$ required to produce a fluence of one Roentgen as a function of photon energy.

## Ionization Chambers: Beam Monitors for Fast Neutrons

Fast neutrons used in medical radiotherapy treatments have ranged in energy from 5-50 MeV. On the assumption that the incident fast neutron beam is collimated by a suitable entrance channel, it is possible to use appropriate ionization chambers to monitor the neutron flux as shown in Fig. 1. For this purpose, a standard parallel-plate ionization chamber with suitable guard rings can be used when filled with a suitable gas, such as methane at 1-10 atmospheres pressure. The ionization current is produced by the n-p elastic interaction with the hydrogen atoms in the gas. Since the maximum intensity of fast neutron fluxes is approximately $10^{11}$-$10^{12}$ neutrons/$cm^2$/sec, there is little risk of non-linearities due to saturation. In principle, since the elastic n-p cross section is well known at these energies and the recoil spectrum of the protons easily calculable, the energy deposited in the sensitive region of the ion chamber can be determined quite accurately. At the higher neutron energies, the interaction with the walls and the carbon atoms has to be taken into account.

In summary, ionization chambers of the parallel-plate type with suitable precautions to eliminate leakage currents by guard rings and other devices can be used as absolute monitors for collimated beams of the radiations discussed here. In practice, since absolute

devices must be maintained very carefully, including the readout and charge integrating electronics, it is advisable to maintain some secondary standards against which their calibration can be checked periodically.

## Gas-filled Detectors: Proportional and Geiger Counters

The ionization chambers described in the previous sections are suitable for monitoring large fluxes of radiation (more than $10^6$ charged particles/sec) by measuring the current produced in the chamber by some suitable electrometer.

The proportional counters and Geiger counters described in this section are capable of detecting single charged particles and recording the energy deposited/particle in the counter. As beam monitoring devices, they have to be used with beam fluxes of less than $10^7$ charged particles/sec for a proportional counter or less than $10^5$/sec for a Geiger counter.

The ability to detect single particles is due to the internal gas amplification of the primary charge deposited in the counter sensitive volume by the passage of a charged particle. Gas amplification occurs in electric field regions which are large enough to cause primary electrons to ionize successive gas atoms before collection. High electric fields at low voltages are obtained by making the detectors cylindrical in shape with the anode consisting of a small diameter wire. Typical dimensions for these counters are: anode wire 20-50 microns diameter; cathode diameters range from a few mm to several cm. From electrostatics, the electrical field in a cylindrical configuration is

$$E(r) = \frac{V}{r \ln b/a}$$ ; V = applied potential, a = anode wire radius, b = cathode inner radius.

From this formula it can be seen that for applied potentials of 1,000-2,000 volts, electric fields of the order 100-300 KV/cm can be readily obtained at distances of a few anode wire radii, which is the region where most of the avalanche gain takes place.

Fig. 5a shows a typical construction of an avalanche gain detector. The distinction between a proportional and Geiger counter can be understood from the avalanche gain versus applied voltage graph of Fig. 6b. At low voltages, the electric field is sufficient to collect all the primary electrons and ions: this is the ionization regime. At higher voltates there is some avalanche gain which increases with voltage. At still higher voltages, there are charge collection saturation effects, and the avalanche gain is no longer

proportional to the number of primary electrons. A small voltage region between this point and breakdown is the Geiger region, where an input pulse of any amplitude produces the same saturated output pulse of approximately $10^8$ electrons.

The characteristics of these counters depend strongly on the gas filling. Since the avalanche gain is produced by electrons, it is necessary to use gases that are not electronegative, i.e. do not capture free electrons to form negative ions. Suitable gases for this purpose are the noble gases He, Ar, Ne, Kr and Xe. All of these gases have metastable states which emit photons in the ultraviolet, and therefore the possibility exists that they can start secondary discharges by ejecting photoelectrons from the cathode walls. In order to prevent this, it is necessary to add a small admixture, typically 5-10% of a "quenching gas," which is usually a non-electronegative polyatomic gas with strong absorption in the ultraviolet. Typical quenching gases are saturated hydrocarbons, methane, ethane, isobutane, alcohol and inorganic gases, such as $CO_2$.

There is an extensive literature on the properties of proportiona and Geiger counters and the detailed mechanisms of the quenching action of the various gas mixtures.

Figs. 5b and 5c show a modern development of the cylindrical proportional counter, called the MWPC (Multiwire Proportional Chamber). These devices are used extensively in physics research when it is necessary to cover large areas with proportional counters with a minimum amount of absorbing or scattering material. As shown in Fig. 5d, a set of parallel anode wires produces electric field equipotentials and gradients in the immediate vicinity of each wire similar to those in cylindrical proportional counters. Thus, a local avalanche region is formed at each wire. By good design, it is possible to ensure uniformity of response over areas of a few square meters.

For our purposes in this review, we note the following points:

1) For charged particle detection, these counters can be filled with any noble gas-quenching gas mixture that produces satisfactory electrical signals.

2) Neutron counters, in which the neutrons are detected by their interaction with the specific filling of the chamber to yield an ionizing particle, require special gas mixtures containing $^3He$ or $BF_3$. An alternative approach is to coat the inner surface of the cathode with a boron or lithium compound.

3) Proportional counters are used if there is any need to

Table III. Properties of Neutrons:
Gas-filled Neutron Detectors

| | |
|---|---|
| Thermal Neutron: | Slow neutron $E_n$ = 0.025 eV<br>Capture in matter → gamma rays |
| Fast Neutron: | Anything above 10 keV<br>Radiotherapy range 5-50 MeV<br>Capture in matter → charged particles<br>→ gamma rays |
| Thermal Neutrons: | Reactions with high capture probility yielding highly ionizing charged particles: exothermic reactions. |
| | $n + {}^{10}_{5}B \rightarrow {}^{6}_{3}Li + {}^{4}_{2}He$ $\quad E_\alpha$ = 2.79 MeV |
| | $n + {}^{3}_{2}He \rightarrow {}^{3}_{1}He + {}^{1}_{1}H$ $\quad E_p$ = 0.57 MeV |
| | $n + {}^{6}_{3}Le \rightarrow {}^{4}_{2}He + {}^{3}_{1}H$ $\quad E_H$ = 2.73, $E_\alpha$ = 2.05 MeV |
| | $n + {}^{235}_{92}U \rightarrow$ Fission $\quad$ E(fission fragments) 150 MeV |
| Fast Neutrons: | Reactions with interaction probability. Elastic scatter or break-up into charged particles. |
| | $n + {}^{1}_{1}H$ (hydrocarbons) → Hydrogen recoils |
| | $n + {}^{238}_{92}U$ ($^{232}_{90}Th$) → Fission fragments |

discriminate between different types of radiation incident on the chamber by the magnitude of the ionizing energy retained within the sensitive volume of the counter.

4) Proportional counters can operate at higher speeds than Geiger counters, typically up to $10^7$ cts/sec versus less than $10^5$/sec for the Geiger counters.

5) Geiger counters produce very large uniform pulses which can be scaled by very simple electronics; hence, they are often used in survey meters and other portable monitoring instruments.

Table V. Characteristics of TL Phosphors

| Characteristic | LiF | $Li_2B_4O_7$:Mn | $CaF_2$:Mn | $CaF_2$:nat | $CaSO_4$:Mn |
|---|---|---|---|---|---|
| Density (g/cc) | 2.64 | 2.3 | 3.18 | 3.18 | 2.61 |
| Effective atomic number | 8.2 | 7.4 | 16.3 | 16.3 | 15.3 |
| TL emission spectra ( ) | | | | | |
| a) range | 3500-6000 | 5300-6300 | 4400-6000 | 3500-5000 | 4500-6000 |
| b) maximum | 4000 | 6050 | 5000 | 3800 | 5000 |
| Temperature of main TL glow peak | 195°C | 200°C | 260°C | 260°C | 110°C |
| Efficiency at $^{60}Co$ (relative to LiF) | 1.0 | 0.3 | 3 | ~23 | ~70 |
| Energy response without added filter (30 KeV/$^{60}Co$) | 1.25 | 0.9 | ~13 | ~13 | ~10 |
| Useful range | mR-$10^5$ R | mR-$10^6$ R | mR-$3x10^5$ R | mR-$10^4$ R | μR-$10^4$ R |
| Fading | Small, <5%/12 wk | ~10% in first mo. | ~10% in first mo. | No detectable fading | 50-60% in first 24 hrs. |

Table VI. Composition and Dosimetric Properties of Some Radiophotoluminescent Dosimeter Glasses

| Author (Manufacturer) | Composition (% by weight) | | | | | | Pre-dose in rad γ equivalent (approx.) | Relative γ-sensitivity (approx.) | Effective atomic number | Energy dependence: 50 keV / 1 MeV (calculated) |
|---|---|---|---|---|---|---|---|---|---|---|
| | Ag | Al | Li | P | O | Others | | | | |
| Schulman et al. (1951) (Bausch & Lomb High-Z) | 4.3 | 4.7 | | 28.4 | 44.1 | 10.8 Ba<br>7.7 K | 10.0 | 1.0 | 28.0 | 32.0 |
| Ginther and Schulman (1960) (Bausch & Lomb Low-Z) | 4.3 | 4.7 | 1.9 | 33.7 | 52.3 | 3.1 Mg | 10.0 | 1.0 | 17.6 | 10.0 |
| Yokota et al. (1961) (Toshiba) | 4.2 | 4.6 | 3.6 | 33.3 | 53.5 | 0.8 B | 0.2 | 2.2 | 17.5 | 10.0 |
| Francois et al. (1965) (C.E.C.) | 2.4 | 3.5 | 2.5 | 33.8 | 52.5 | 0.5 Be<br>4.7 Na | 0.7 | 1.9 | 15.4 | 7.3 |

Gas-filled Detectors: Detection of Thermal and Fast Neutrons

In a previous section we noted that hydrocarbon gas-filled ionization chambers of conventional construction could be used for monitoring large fluxes of fast neutrons. The detection mechanism in that case was the ionization current produced by the proton recoils.

In this section we describe some gas-filled detectors particularly suitable for use as neutron detectors. The type of detector depends on whether it is intended for thermal neutrons ($E_n$ = 0.025 eV) or for fast neutrons. In any application of fast neutrons, such as Neutron Radiotherapy ($E_n$ = 5-50 MeV), it should be remembered that the background radiation flux in any concrete-shielded area is due to the primary fast neutrons and also to the thermalized neutrons from the slowing-down interactions in the walls.

For thermal neutron detection, it is necessary to use a gas filling or wall coating of some element which yields an energetic charged particle with a high interaction probability which then ionizes the counter gas. In Table III we list some thermal neutron capture reactions which are extensively used in various neutron detectors.

Standard thermal neutron proportional counters are made with $BF_3$ or $^3He$ gas fillings. The proportionality feature of the counter is used (Fig. 6a) in allowing the scalers, which count the individual pulses, to discriminate between a thermal neutron indirect pulse and a gamma ray pulse from the high flux of gamma rays that is usually present in a thermal neutron ambience.

Another ionizing reaction that is characteristic of neutrons, thermal and fast, is the fission process in heavy elements. Fig. 6b shows the fission cross section for $^{235}U$, $^{239}Pu$, $^{238}U$ and $^{237}Np$. $^{238}U$ and other even isotopes of uranium and thorium are fast neutron fission isotopes.

Since the charged fragments from the fission process release an energy of approximately 80 MeV/fission fragment, the ionization pulse is large enough so that avalanche gas gain is not needed and a parallel-plate ionization chamber can be used in a pulse mode. A fission neutron detector is shown in Fig. 6c. It consists of a large number of thin metal plates coated on both sides with a thin deposit of the appropriate uranium or other heavy element isotope. The maximum thickness of the deposit has to be small enough so that the pulse height from a fission fragment which has to traverse the entire thickness of the plating emerges into the gas volume with a sufficient energy to be detected above the amplifier noise and the pulses from alpha particles, which usually occur in the spontaneous

decay of the trans-uranium isotopes. Note that all the high-voltage plates are mounted on one set of insulating rods and ground plates on another set: this is a form of guard ring configuration to prevent electrical leakage signals.

In Figs. 7 and 8 we show two configurations of fast neutron detectors in which the detector element itself is basically a thermal neutron counter: a $BF_3$- or $^3He$-filled proportional counter. The fast neutrons are slowed down in a surrounding hydrogenous $CH_2$ plastic envelope and detected with high efficiency by the central detector when thermalized.

The counters shown in Fig. 7 are called Bonner spheres: they are made with various diameter $CH_2$ spherical blankets. The sensitivity of various Bonner spheres versus neutron energy is shown in Fig. 7b. These spherical detectors were intended initially for use in estimating the energy distribution of a flux of fast neutrons by comparing the counting rates of the various diameter spheres. From the known sensitivities it is possible to calculate a rough energy spectrum.

The interest to neutron dosimetry of this type of counter is illustrated in Fig. 7c, which shows the sensitivity-versus-neutron energy response of the 10-inch (25.4 cm) sphere and the relative equivalent dose per neutron; the two curves are sufficiently close so that dose measurements can be done by use of this particular diameter Bonner detector.

Another approach to fast neutron detection for an unknown distribution of neutron energies is to design a hydrocarbon-moderated detector whose response is the same over a wide range of neutron energies. Counters of this type, known as long counters, are shown in Fig. 8. In Figs. 8a and 8b we show an earlier version of a long counter with a single $BF_3$ proportional detector at the center. A flatter response curve is obtained with the more complicated long counter, shown in Fig. 9a and 9b, using multiple $^3He$ detectors.

## Thermoluminescent (TLD) and Radiophotoluminescent Detectors (RPL)

The interaction of radiation with matter in crystalline and amorphous forms produces a variety of deformations which can be used as a measure of the intensity of the incident radiation. Some interactions with crystalline matter are shown in Table IV. From this list the thermoluminescent and radiophotoluminescent phenomena have turned out to be particularly suitable for dose measurements in the useful medical range, i.e. from a few mrads to thousands of rads.

Thermoluminescent detectors. The thermoluminescence process

Table IV. Summary of the Types of Solid State Systems Used for Dosimetry

| Type of centers produced | Measured parameter | Material |
|---|---|---|
| Centers stable with respect to readout. | A. Coloration | 1. Glasses<br>2. Plastics<br>3. Dyes |
| | B. Radiophotoluminescence | Phophate glass |
| | C. Degradation of luminescence | Anthracene, etc. |
| | D. Electron spin resonance | Alanine |
| Centers destroyed by measurement | A. Thermoluminescence | 1. $CaSO_4$:Mn<br>2. $CaF_2$:Mn<br>3. LiF |
| | B. Infrared-stimulated luminescence | SrS:Eu, Sm |

can be understood in terms of Figs. 10a and 10b. Fig. 10a shows the electronic energy diagram of an ionic crystal. Radiation can eject an electron from the filled valence band to the conduction band, resulting in an electron and hole which are both mobile. If these are collected by external connectors, we have a semiconductor detector. However, as shown in Fig. 10b, the crystal may have a small concentration of another element that forms energy levels which act as trapping centers for both the electrons and holes released by the radiation. By suitable choice of crystal and impurity element, these trapping centers may, under the action of heat, cause the electron to be released from its trapped level and cause recombination with the hole. The energy released is often in the form of a photon in the visible region.

A variety of inorganic crystals with these suitable properties exists, as shown in Table V. From this table it can be seen that

all of these crystals can be used for radiation dosimetry in the medically useful range. Fig. 11a shows the response as a function of x-ray or gamma ray energy of LiF and $CaF_2$ doped with Mn. The flatter response curve of the LiF for incident x-ray energy below 200 KeV is one reason for its wide use as an x-ray dosimeter. The response curve to other forms of radiation will not necessarily have the same shape, and hence other TLD crystals may be equally useful.

LiF can be used as a dosimeter for thermal neutrons by use of $^6$LiF crystals; the response of the dosimeter is then due to the ionization produced in the crystal by the exothermic proton from the neutron capture reaction. The Health Physics group at the Lawrence Berkeley Laboratory has also used LiF dosimetry in heavy ion beams and calibrated their response relative to x-rays.

The thermoluminescent material, in the form of a powder, small rods or powder extruded into teflon plastic discs, is read out by heating it in an opaque enclosure. A photomultiplier tube built into the enclosure records the amount of light released, which is proportional to the integrated flux of radiation to which the crystals have been exposed. Fig. 11b shows a typical light emission curve (glow curve) of a thermoluminescent crystal ($CAF_2$:Mn) as a function of heater temperature. LiF and other crystals have very similar curves, each peaking at slightly different temperatures.

Radiophotoluminescence (RPL) detectors. Although the RPL phenomenon has been known since 1912, its theoretical basis is not completely understood. In silver-activated phosphate glass, ionizing radiation produces two effects: (1) it increases the optical density over a broad wavelength region in the ultraviolet and the visible, and (2) it forms stable fluorescing centers that emit orange light (500-700 nm) under ultraviolet excitation (365 nm). These fluorescence centers are due primarily to silver deposits in the form of $Ag^{2+}$ ions formed from the $Ag^{+}$ ions of the crystal by loss of an electron. There are other effects which contribute to the fluorescence. Fig. 12a shows a schematic diagram of an RPL reader and Fig. 12b shows typical absorption and luminescence curves of an RPL glass.

In Table VI we show some properties of commonly used RPL glasses. Fig. 13a shows, for various RPL glasses, the minimum dose that can be measured, relative sensitivity, mean atomic number, and response as a function of gamma ray energy. Fig. 14b shows the fading effect of the RPL response with time. If we accept a basic accuracy of $\pm$10%, then all the RPL glasses listed here are satisfactory from a few minutes after exposure to over 100 days.

Both TLD and RPL dosimeters are coming into wide use and displacing film as dosimeters for personnel working in laboratories

where there is some radiation exposure. They are both used also as patient dosimeters in Radiation Therapy exposures.

## SCINTILLATION DETECTORS

The scintillation process was used in the earliest experiments in alpha particle counting by Rutherford and his group in the early 1900's, using ZnS as the scintillator and the human eye as the the detector. After being supplanted in 1919 by the invention of the Geiger counter, it came into use again in particle physics around 1950, following the development of the photomultiplier tube some years earlier, and with the discovery by Kallman that various organic crystals with a cyclic structure that were previously known to fluoresce strongly under ultraviolet radiation were capable of emitting photons in the visible range under the action of ionizing particles. Since then, the scintillation detector has come into wide use in particle physics research, radioactive tracer work, and gamma ray spectroscopy. Scintillation counters are not used very much in radiation dosimetry, primarily because their gain sensitivity is too variable compared to the other detectors discussed here.

In Fig. 14a we show a basic scintillation detector. The scintillator material is mounted directly on the face of the P-M tube. Fig. 14b shows a flat scintillator optically coupled to the P-M tube by polished plastic light pipes in step form. In actual use, the scintillator light pipes and P-M tubes would be enclosed in light-tight wrapping. Fig. 14c shows the dynode structure of other types of P-M tubes than that shown in Fig. 15a. All the P-M tubes have a photocathode whose response is selected to match the light emission of the scintillator material and whose cathode efficiency ranges from 20-30%. The multiplication process takes place in the evacuated glass container, where the dynodes are located. By applying suitable potentials to the dynode, an individual electron from the photocathode is accelerated to the first dynode where it releases a small number (3-5) of secondary electrons. Each of these electrons in turn releases more secondary electrons from the next dynode until the final pulse of electrons is collected in a metallic collection box. Depending on the number of dynodes in a P-M tube and the applied potential across them, gains between $10^5$-$10^8$ can be achieved. The photocathodes are also made with different sensitivity peaking at different wavelengths from 700-300 nm.

Since 1950, many different types of scintillators have been developed for detector applications. The low Z scintillating $C_nH_m$ compounds are generally used in solutions or polymerized into a plastic binder. The liquid scintillators are used extensively for accurate counting of radioactive tracers. The plastic scintillator

is the most widely used type for particle counting, for beam monitoring, and for low-energy gamma ray counting. The ability to shape the plastic to any desired form makes it universally useful. The general requirement for an organic scintillator, in crystalline, solvent or plastic polymerized form is that its optical absorption bands and emission bands should not overlap. Table VII lists various scintillation materials which can be used as crystals in solutions or in plastics.

Table VIII summarizes some of the properties of inorganic crystals. The main interest in the inorganic crystals is that they can contain specific elements of interest for neutron or gamma detection and spectrometry. Fig. 15a explains schematically the properties of a scintillating inorganic crystal. Non-overlap between the absorption and emission wavelengths is achieved by adding small amounts of selected impurities to various transparent cyrstals. These activation compounds create suitable levels in the forbidden gap. The process is very similar to the thermoluminescence activation. The main difference is that in these crystals the activator-excited states release their energy rapidly ($10^{-6}$ sec or faster) in order to allow the crystals to be used with fast-counting electronics. These scintillators have to be used in crystalline form; it is not possible to have the versatility of using them in solution or in plastics. This is due, of course, to the fact that the crystal lattice and energy levels are essential for the light emission process. Fig. 15b shows that the light emission bands of the crystals listed here are a suitable match to the photomultiplier tubes.

For neutron detection, the crystal $^{6}$LiI(Eu), with good scintillation properties, is available. $^{6}$Li-loaded glasses and $^{10}$B-loaded glasses are available also for neutron detection. The main use of the inorganic scintillators has been for gamma ray detection and gamma spectroscopy, where the fact that some of them have high Z elements means that their interaction probability is many orders of magnitude higher than for the CH compounds. Until recently, the almost universally used gamma detector has been the NaI (various activators) crystal. During the last few years a new crystal, Bismuth Germanate ($Bi_4Ge_3O_{12}$), has been developed and is coming into use. The main advantage of this crystal is that it contains bismuth, whose higher Z, relative to that of the iodine, makes it more sensitive to gamma ray interactions. It has a defect in that its light output is approximately 10% that of a comparable NaI crystal.

In summary, the scintillation counters have been the most widely used detectors in research in Radiation Physics and applications of radiation to biology and chemistry. Their easily-controlled gain response, although an asset in a research environment, is probably a drawback for a medical environment where long-term stability is more important.

Table VII. Organic Scintillators

| Scintillator | Density ρ (gm/cm$^3$) | Effective atomic number Z | Wavelength of max. emission (nm) | Refractive index | Light yield relative to anthracene | Decay time (nsec) |
|---|---|---|---|---|---|---|
| Anthracene | 1.25 | 5.8 | 445 | 1.59 | 1.00 | 25 |
| Quarter-phenyl | --- | 5.8 | 438 | --- | 0.85 | 8 |
| Stilbene | 1.16 | 5.7 | 410 | 1.62 | 0.73 | 7 |
| Terphenyl (para) | 1.12 | 5.8 | 415 | --- | 0.55 | 12 |
| Diphenyl-acetylene (Tolan) | 1.18 | 5.8 | 390 | --- | 0.26-0.92 | 7 |
| Naphthalene | 1.15 | 5.8 | 345 | 1.58 | 0.15 | 75 |

Table VIII. Properties of Inorganic Scintillators

| Material | Wavelength of Maximum Emission (nm) $\lambda_m$ | Decay Constant (μs) | Index of Refraction at $\lambda_m$ | Specific Gravity | γ Scintillation Efficiency Relative to Na(Tl) |
|---|---|---|---|---|---|
| NaI(Tl) | 410 | 0.23 | 1.85 | 3.67 | 100% |
| CsI(Na) | 420 | 0.63 | 1.84 | 4.51 | 85 |
| CsI(Tl) | 565 | 1.0 | 1.80 | 4.51 | 45 |
| $^6$LiI(Eu) | 470-485 | 1.4 | 1.96 | 4.08 | 35 |
| ZnS(Ag) | 450 | 0.20 | 2.36 | 4.09 | 130 |
| CaF (Eu) | 435 | 0.9 | 1.44 | 3.19 | 50 |
| $Bi_4Ge_3O_{12}$ | 480 | 0.30 | 2.15 | 7.13 | 8 |
| CsF | 390 | 0.005 | 1.48 | 4.11 | 5 |
| Li glass | 395 | 0.075 | 1.55 | 2.5 | 10 |

REFERENCES AND ACKNOWLEDGMENTS

The material for this lecture has been obtained from various Lawrence Berkeley Laboratory reports written by staff members of the Health Physics and Biophysics groups. I have also made extensive use of graphs and information from the following textbooks:

1) F. H. Attix, W. C. Roesch and E. Tochlin, "Radiation Dosimetry" (2nd ed., New York: Academic Press, 1966), II and III.
2) W. J. Price, "Nuclear Radiation Detection" (2nd ed., New York: McGraw-Hill Book Co., 1964).
3) N. W. Holm and R. J. Berry, "Manual on Radiation Dosimetry" (New York: Marcel Dekker, Inc., 1970).
4) G. F. Knoll, "Radiation Detection and Measurement" (New York: John Wiley & Sons, 1979).



I would like to take this opportunity to thank for following members of the Lawrence Berkeley Laboratory staff, whose assistance is deeply appreciated: R. H. Thomas, J. McCaslin, J. Howard, A. Smith, P. Wiedenbeck and C. Johnson-Joy.

This work was supported by the Physics Research Division of the United States Department of Energy under contract no. W-7405-ENG-48.

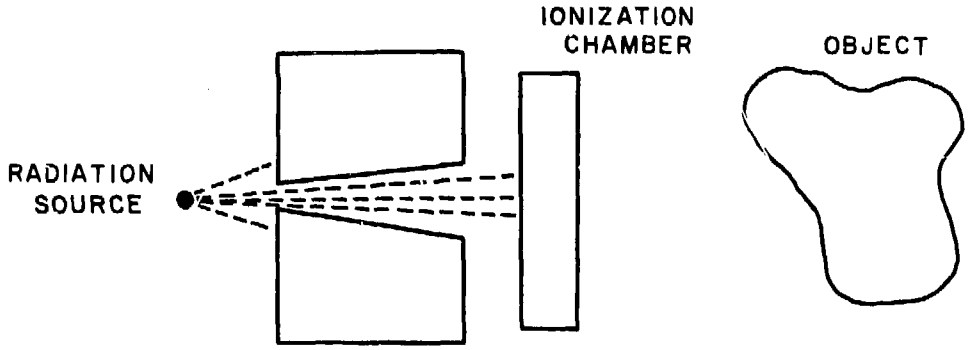


Fig. 1a. Beam-monitoring from a collimated source.

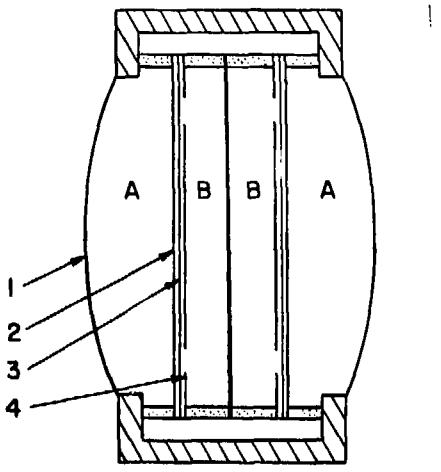


Fig. 1b. Parallel-plate ionization chamber with guard rings.

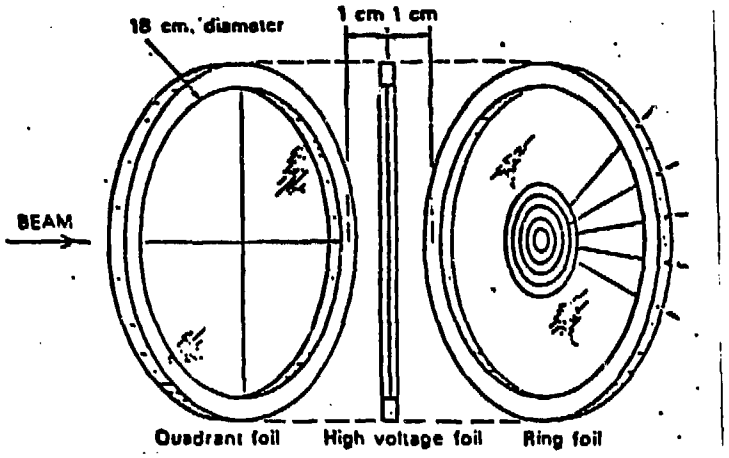


Fig. 1c. Parallel-plate ionization chamber for beam centering with quadrant or annular collector foils.

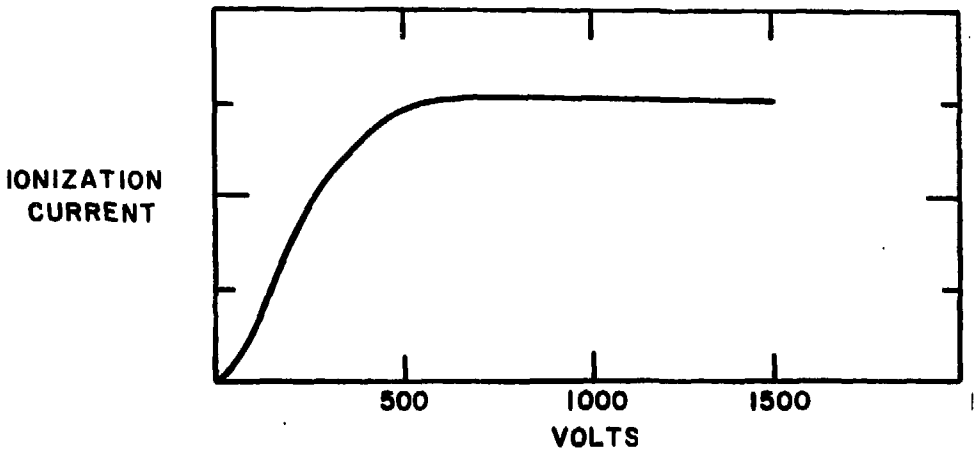


Fig. 1d. Ionization chamber collector voltage plot for chamber, showing plateau region.

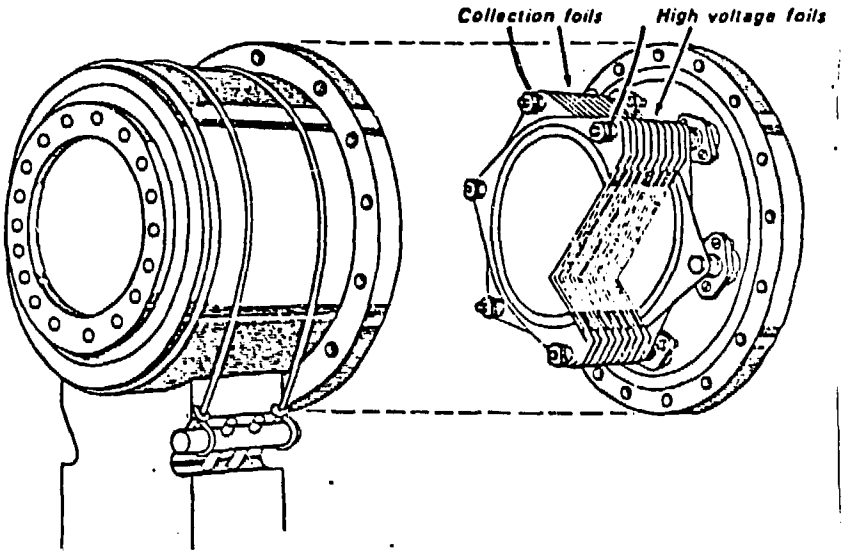


Fig. 2a. Exploded view of secondary electron beam monitor. Reprinted with permission of Academic Press, Inc., copyright 1966.

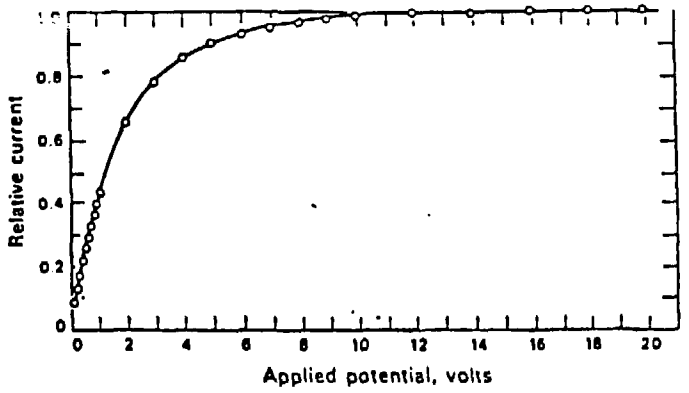


Fig. 2b. Secondary electron current - collector voltage plot. Reprinted with permission of Academic Press, Inc., copyright 1966.

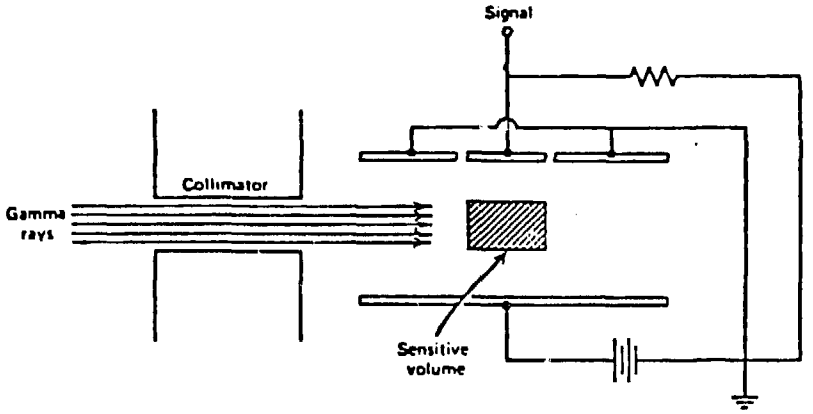


Fig. 3a. Free-air ionization chamber showing guard-ring defined sensitive volume.
Reprinted with permission of John Wiley & Sons, Inc., copyright 1979.

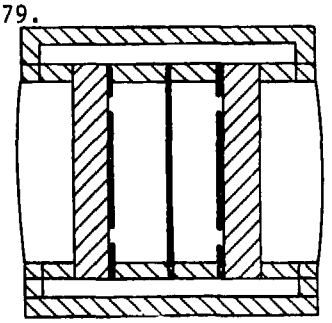

Fig. 3b. Air equivalent ionization chamber with wall thickness compensation

| Photon Energy (MeV) | Thickness ($g\ cm^{-2}$) |
|---|---|
| 0.02 | 0.0008 |
| 0.05 | 0.0042 |
| 0.1 | 0.014 |
| 0.2 | 0.044 |
| 0.5 | 0.17 |
| 1 | 0.43 |
| 2 | 0.96 |
| 5 | 2.5 |
| 10 | 4.9 |

Fig. 3c. Thickness of wall material ($g/cm^2$) for establishment of electronic equilibrium versus photon energy in MeV.

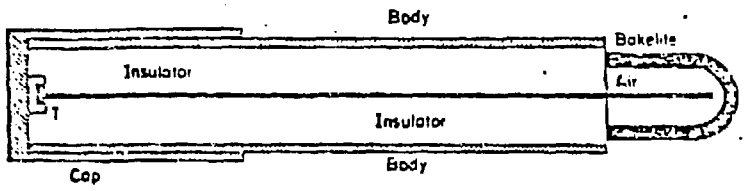


Fig. 3d. Small-volume (thimble) tissue equivalent ionization chamber.

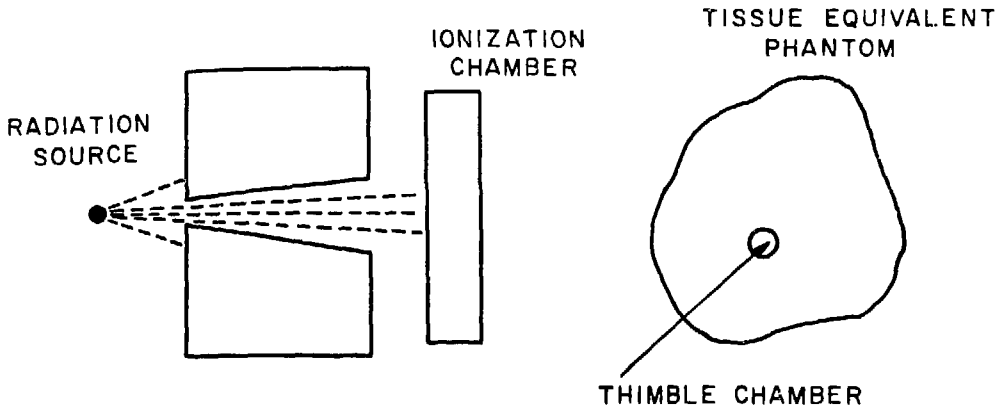


Fig. 4a. Use of ionization chamber to measure incident radiation (Roentgens) and tissue equivalent ionization chamber to measure distribution of absorbed energy in rads.

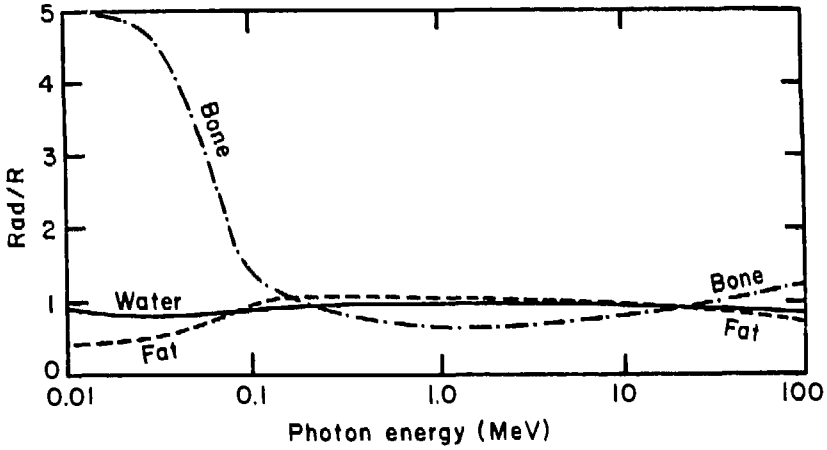


Fig. 4b. Exposure - dose relations for some materials of biological interest.

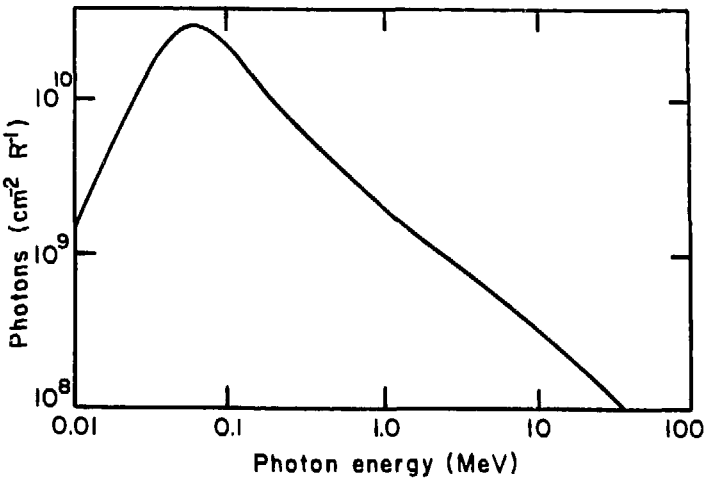


Fig. 4c. Photon number fluence required to produce one rad as a function of photon energy.

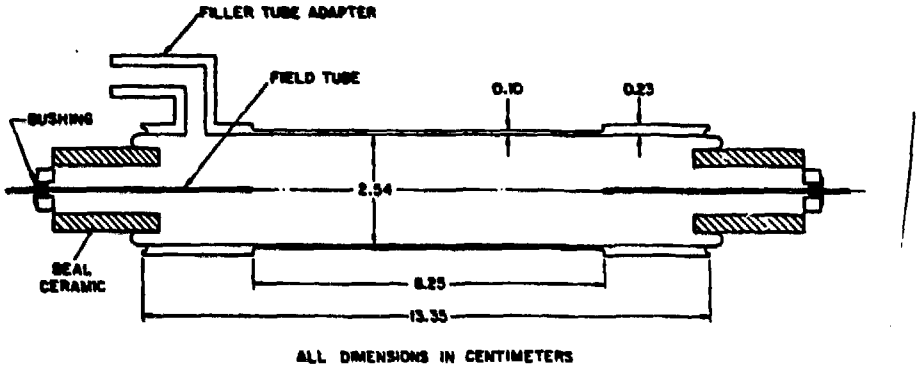


Fig. 5a. Cross-sectional view of proportional chamber showing field tubes that serve as guard electrodes.
Reprinted with permission of John Wiley & Sons, Inc., copyright 1979.

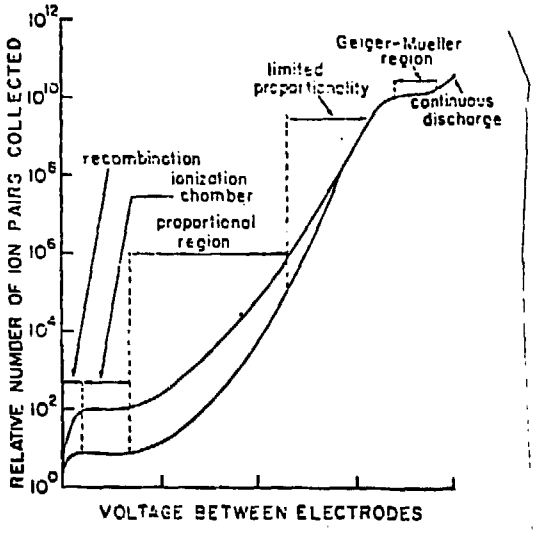


Fig. 5b. Charge multiplication versus voltage for cylindrical proportional counter showing transition from ionization chamber to proportional to Geiger to breakdown conditions.

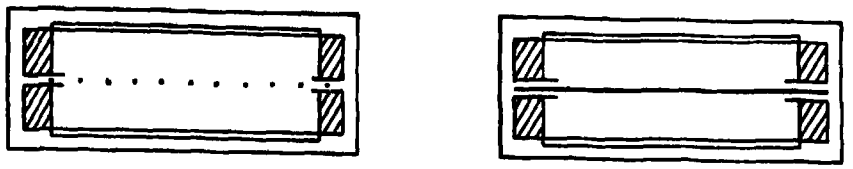

Fig. 5c. Side view of multiwire proportional chamber.

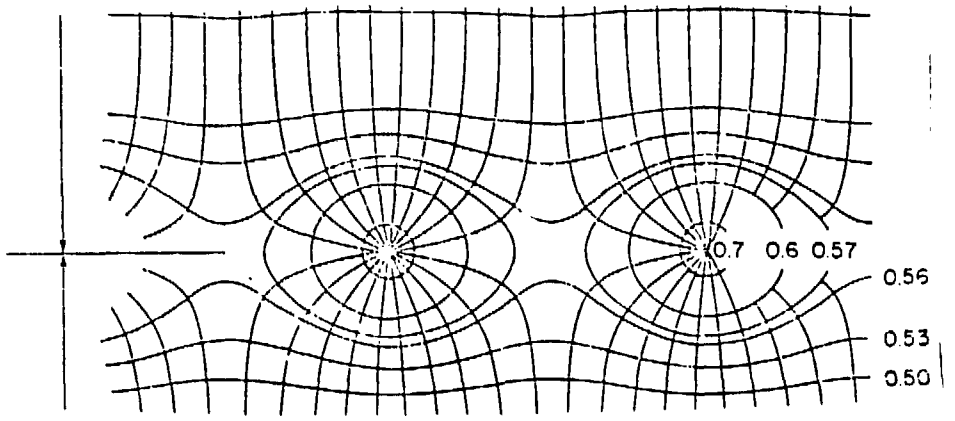


Fig. 5d. Electric field and equipotential distributions in multi-wire proportional chamber.

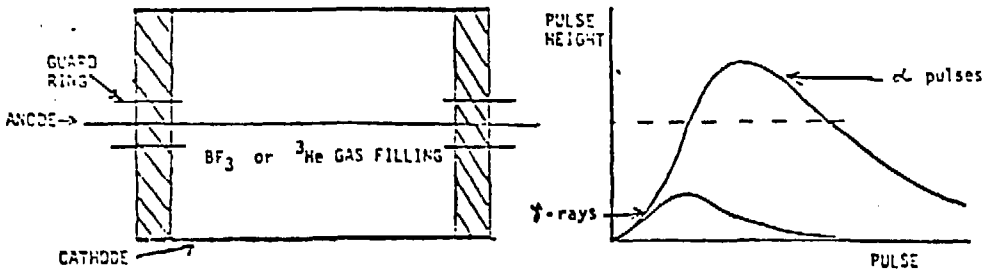


Fig. 6a. Neutron - gamma discrimination by pulse height in $BF_3$ counters.

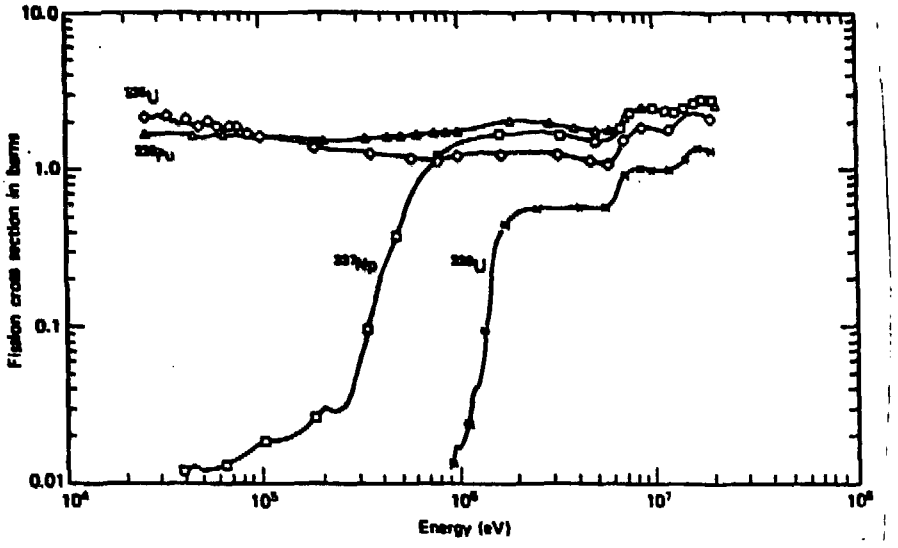


Fig. 6b. Fission cross sections for thermal and fast neutrons for some isotopes used in fission chambers. Reprinted with permission of John Wiley & Sons, Inc., copyright 1979.

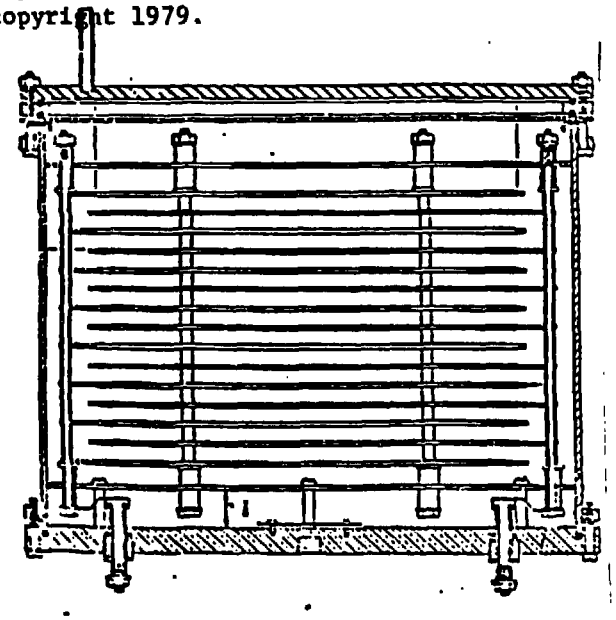

Fig. 6c. Schematic of multiple-plate ionziation fission chamber.

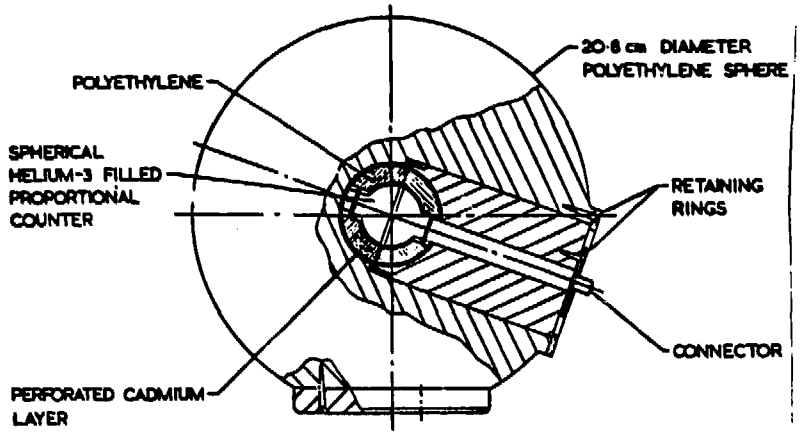


Fig. 7a. Spherical neturon dosimeter based on $^{3}He$-filled proportional counter.
Reprinted with permission of John Wiley & Sons, Inc., copyright 1979.

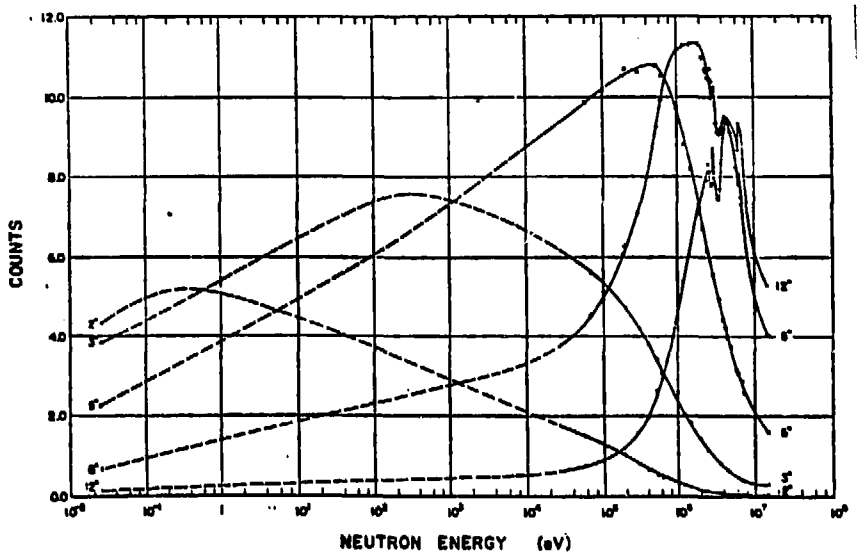


Fig. 7b. Neutron detection efficiency versus neutron energy for spherical Bonner detectors of various diameters.
Reprinted with permission of John Wiley & Sons, Inc., copyright 1979.

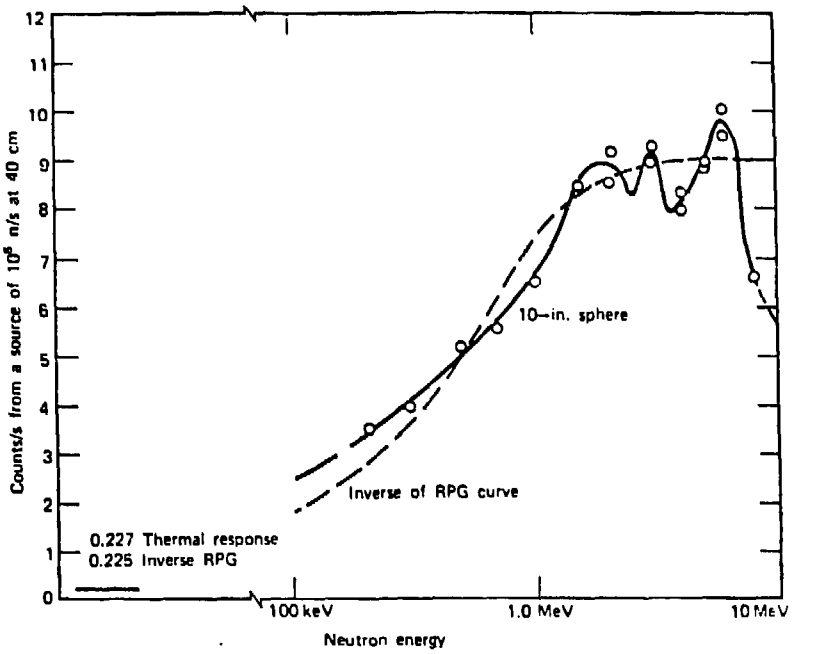


Fig. 7c. Sensitivity of 25.4 cm spherical detector with 4 x 4 mm central detector versus neutron energy. Also shown is the relative dose per nuetron labeled as "inverse of RPG curve." Reprinted with permission of John Wiley & Sons, Inc., copyright 1979.

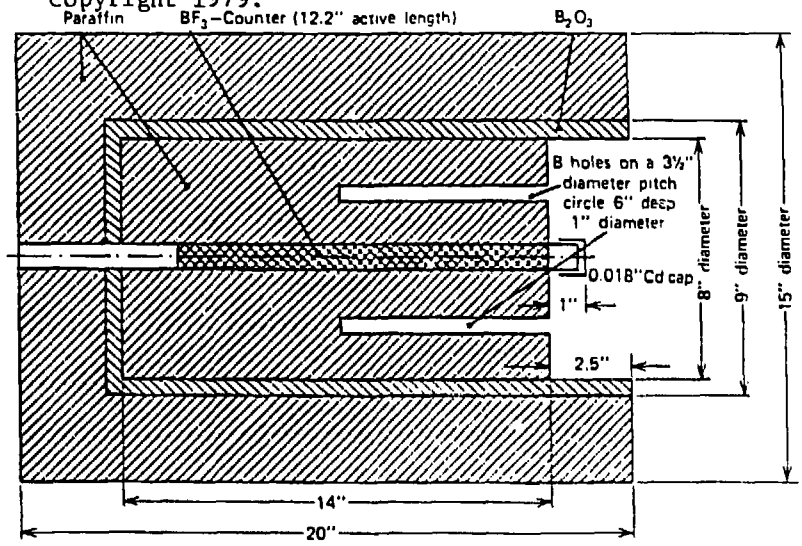


Fig. 8a. Schematic of paraffin-moderated neutron counter with $BF_3$ proportional chamber for detecting the thermalized neutrons.
Reprinted with permission of John Wiley & Sons, Inc., copyright 1979.

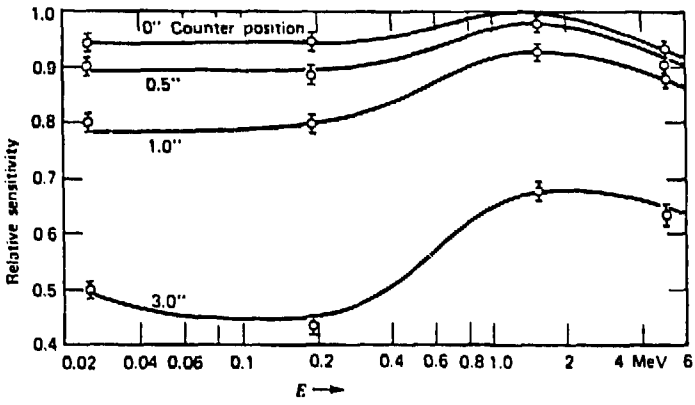


Fig. 8b. Detection efficiency of the counter as a function of neutron energy.
Reprinted with permission of John Wiley & Sons, Inc., copyright 1979.

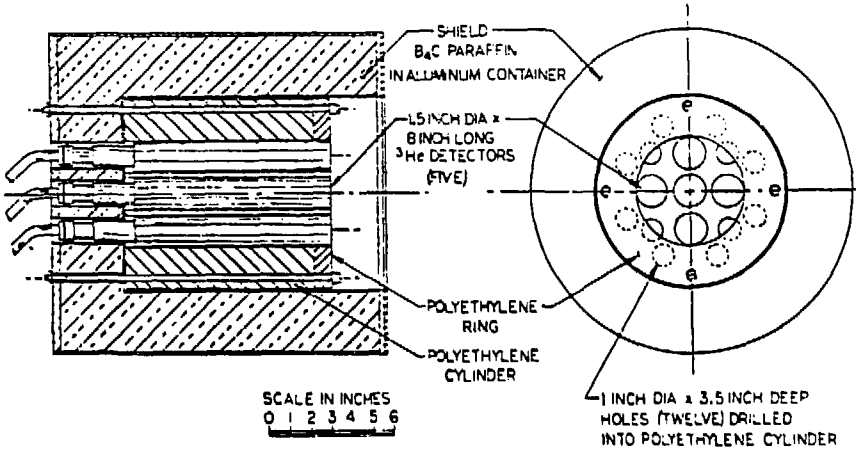


Fig. 9a. Schematic of polyethylene-moderated neutron counter utilizing multiple $^{3}He$-filled proportional counters.
Reprinted with permission of John Wiley & Sons, Inc., copyright 1979.

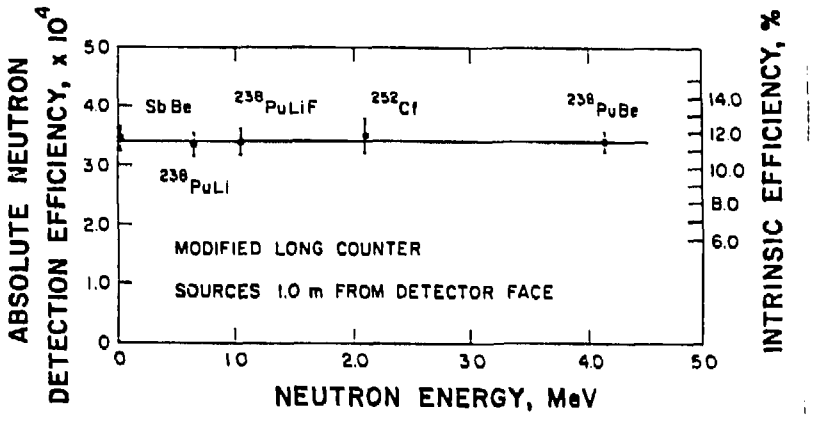


Fig. 9b. Detection efficiency of polyethylene-moderated neutron counter versus neutron energy.
Reprinted with permission of John Wiley & Sons, Inc., copyright 1979.

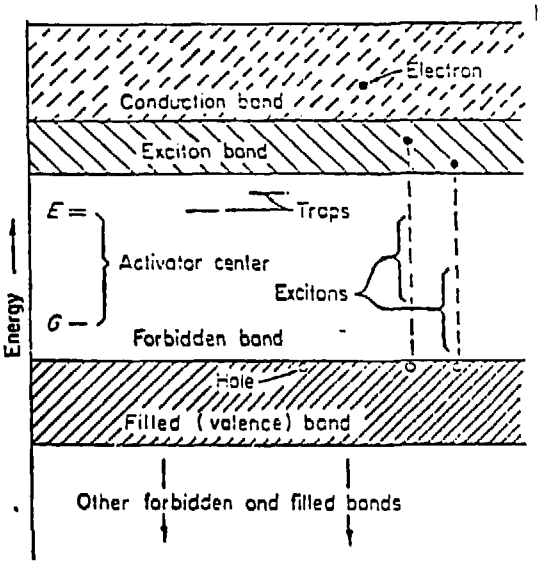


Fig. 10a. Electronic band diagram of an ionic crystal.
Reprinted with permission of Academic Press, Inc., copyright 1966.

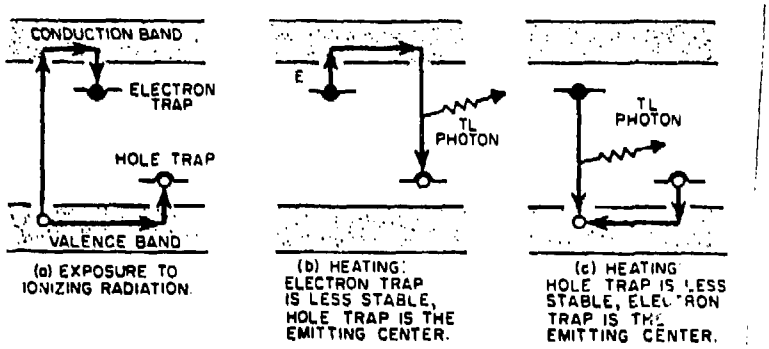


Fig. 10b. Schematic explanation of thermoluminescence. Reprinted with permission of Marcel Dekker, Inc., copyright 1970.

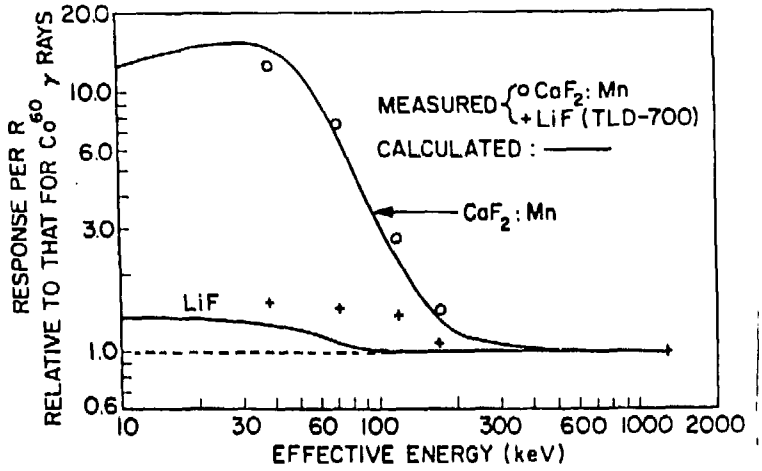


Fig. 11a. Measured and calculated energy dependence of CaF and LiF versus photon energy. Reprinted with permission of Marcel Dekker, Inc., copyright 1970.

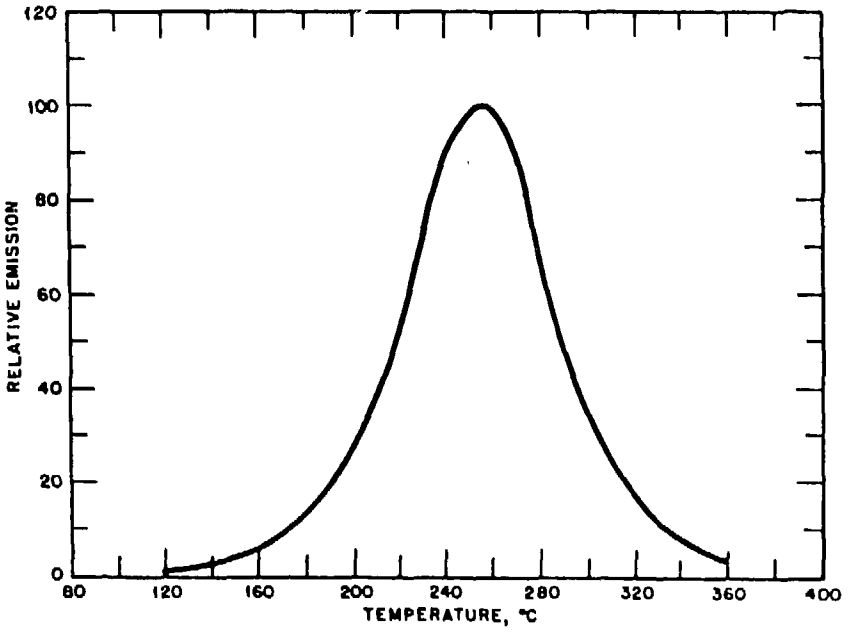


Fig. 11b. Glow curve of CaF dosimeter versus temperature.
Reprinted with permission of Marcel Dekker, Inc., copyright 1970.

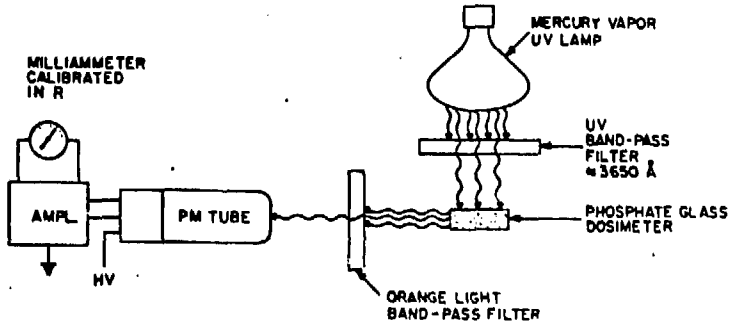


Fig. 12a. Schematic diagram of basic components in an RPL dosimetry reader.
Reprinted with permission of Marcel Dekker, Inc., copyright 1970.

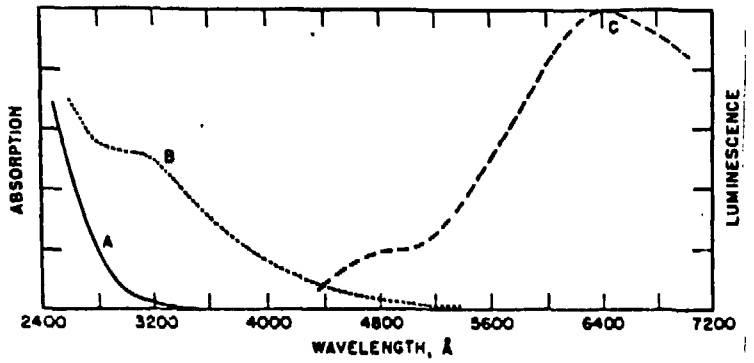


Fig. 12b. Typical absorption and luminescent curves for RPL glass: (A) Absorption band: (B) Emission band. Reprinted with permission of Marcel Dekker, Inc., copyright 1970.

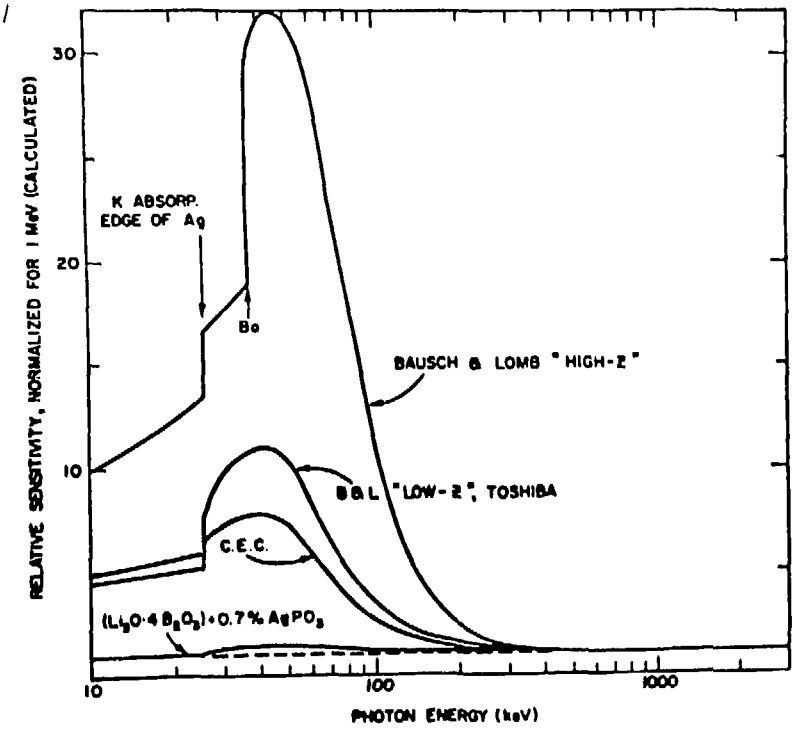


Fig. 13a. Calculated energy dependence of several RPL glasses. Reprinted with permission of Marcel Dekker, Inc., copyright 1970.

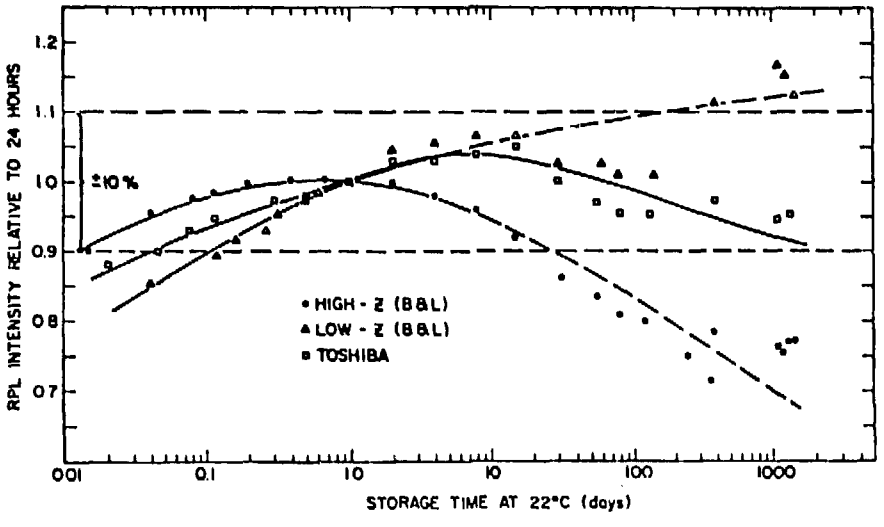


Fig. 13b. Fading characteristics of RPL glasses. Reprinted with permission of Marcel Dekker, Inc., copyright 1970.

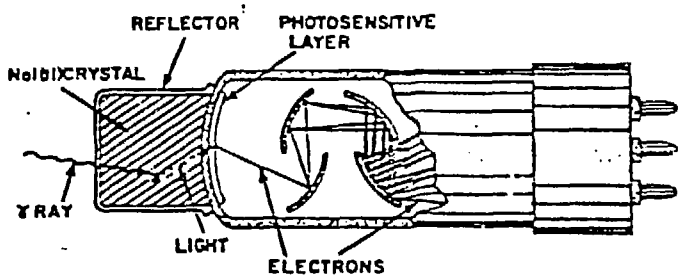


Fig. 14a. Schematic of NaI crystal mounted on photomultiplier.

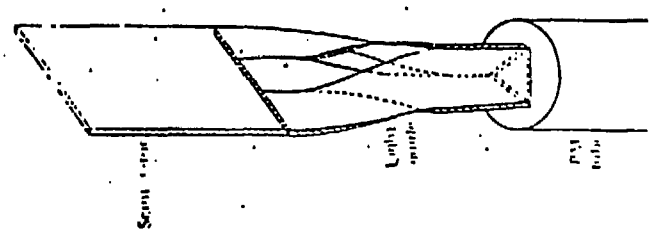

Fig. 14b. Plastic scintillator edge coupled to P-M tube by plastic light guides.

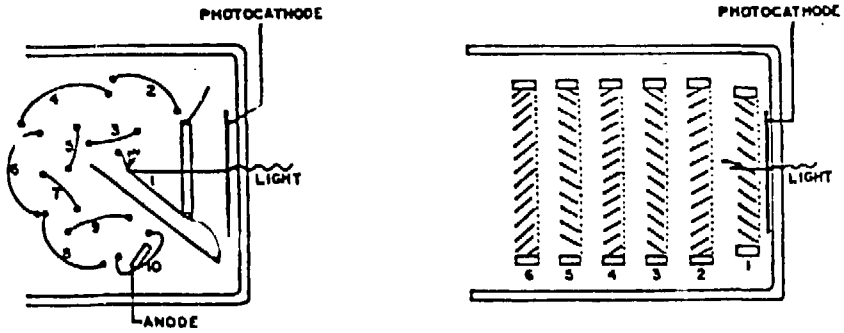


Common photomultiplier tubes. Left, focused electrode tube, and, right, venetian blind tube.

Fig. 14c. Some types of dynode structure in P-M tubes.

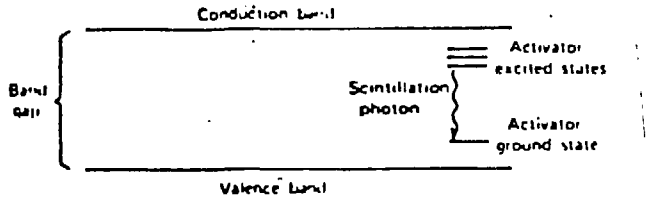


Fig. 15a. Energy band structure of an activated crystalline scintillator.
Reprinted with permission of Academic Press, Inc., copyright 1966.

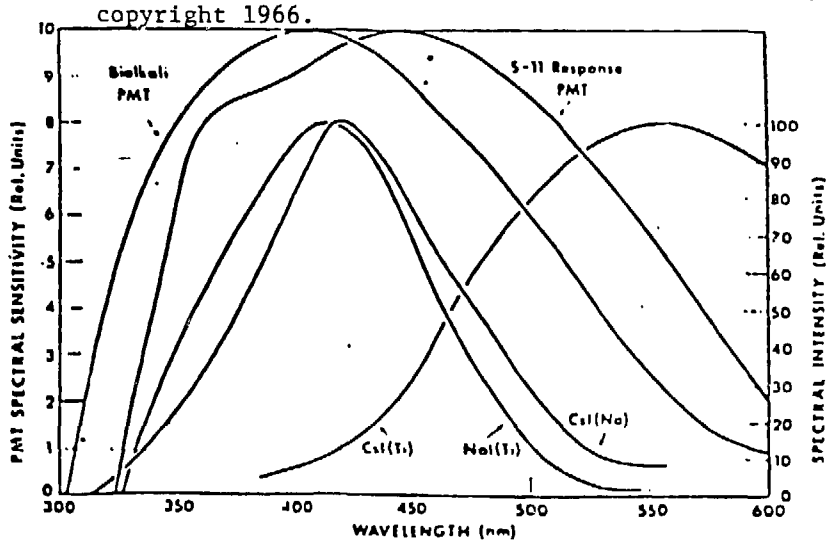


Fig. 15b. Emission spectra of several common inorganic scintillators compared to spectral response of some P-M tubes.
Reprinted with permission of Academic Press, Inc., copyright 1966.